

**Article type:** A-Regular research paper

# Improvement of the quality of short-term forecast of the solar potential using hybrid model: application to Dakar region

**Amy Mbaye<sup>1</sup>, Didier Maria Ndione<sup>3</sup>, Mouhamed Cherif Aidara<sup>1</sup>, Fatou Ndiaye<sup>1</sup>, Amadou Ndiaye<sup>1</sup>, Joseph Ndong<sup>2</sup>, Mamadou Lamine Ndiaye<sup>1</sup>**

<sup>1</sup>Electrical Engineering Department of the Polytechnic High School of Dakar Senegal, Laboratory Head of Water, Energy, Environment, and Industrial Process (LE3PI), BP 5085 Dakar-Fann, Senegal.

<sup>2</sup>Department of Mathematics and Computer Science, University Cheikh Anta Diop of Dakar Senegal, Laboratory LID.

<sup>3</sup>Laboratory of Hydraulic and Fluid Mechanics (HFML), Department of Physics, Faculty of Science and Technology, University Cheikh Anta Diop (UCAD), BP 5005, Dakar-Fann

**Auteur correspondant. E-courrier :** [amy1.mbaye@ucad.edu.sn](mailto:amy1.mbaye@ucad.edu.sn)

RECEIVED: 31 July 2025 / RECEIVED IN FINAL FORM: 02 October 2025 / ACCEPTED: 04 October 2025 in 2025

**Abstract:** This study addresses the critical need to enhance short-term forecasting of solar potential for photovoltaic power generation in Senegal, focusing on the Dakar region. A hybrid forecasting model is developed by integrating a Gaussian Mixture Model (GMM), a Hidden Markov Model (HMM), and a Kalman Filter (KF) to characterize the variability of solar radiation influenced by meteorological factors. The GMM identifies distinct fluctuation states of solar radiation using the EM algorithm, while the HMM captures temporal dependencies between these states through Forward-Backward and Viterbi algorithms. Subsequently, a Kalman Filter refines state-based predictions within a 20-minute horizon. Comparative results demonstrate that the hybrid model [NRMSE=0.0093, NMAE=0.044, and NMBE=0.0006] significantly outperforms the standalone Kalman Filter [NRMSE =0.048, MBE=2.718, and NMAE=0.004], achieving lower normalized root mean square errors and bias metrics. This innovative approach offers a robust probabilistic and deterministic framework to improve intermittent solar energy forecasting, supporting optimized energy planning in the Sahelian zone.

**Keywords:** Solar, Intermittent, Segmentation, Prediction, Hybrid, EM, Viterbi.

**Cite this article:** A. Mbaye, J. Ndong, M.C. Aidara, F. Ndiaye, D.M. Ndione, A. Ndiaye, and M. Ndiaye. Improvement of the quality of short-term forecast of the solar potential using hybrid model: application to Dakar region, OAJ Materials and Devices, Vol 9, 1002-p1 (2025) –DOI: 10.23647/ca.md20251002

## I. INTRODUCTION

The photovoltaic market is expanding worldwide, particularly in Africa and in Senegal. The country's high solar potential has stimulated the rapid deployment of photovoltaic plants, whose production is injected into the national grid operated by SENELEC. Effective integration of these intermittent sources requires detailed spatiotemporal characterization of solar resources. However, their stochastic behavior complicates production–consumption planning. Rapid fluctuations, especially in tropical climates, make forecasting essential.

Reliable forecasting supports assessment, control, and analysis of solar variability. This need motivates the development of a hybrid forecasting model. Hybrid approaches are increasingly explored because individual predictors often perform well only under specific conditions. Prior work notes that deterministic forecasting remains dominant yet limited, as it provides little information on uncertainty [1]–[7]. Probabilistic approaches, now considered more mature and informative [5], [6], help quantify forecasting errors.

Hybrid models combining linear, nonlinear, and probabilistic components have shown improved performance [4], [7]. They compensate for the limitations of individual techniques and enhance prediction accuracy [19]–[21]. Examples include combinations of Kalman Filters with WRF models [22], Markov chains with neural networks [12], [13], and Markov chains with deterministic models [14], [15]. More recently, the Mycielski Markov hybrid model has produced reliable hourly forecasts in Turkey.

This study proposes a hybrid model for forecasting solar radiation in Dakar, Senegal. The approach integrates two probabilistic models (GMM and HMM) with a Kalman Filter. Solar irradiance in the region exhibits multimodal behavior, making GMM suitable for identifying distinct variability regimes via the EM algorithm. GMM also accounts for uncertainty in state classification. However, it does not efficiently capture temporal dependencies between regimes. To address this limitation, an HMM is introduced to model state transitions and compute the most probable sequences [16], [17].

A Kalman Filter, trained using EM, is then applied within each HMM state to extract deterministic components from noisy observations and to refine short-term forecasts [19].

The hybrid model thus highlights fluctuation levels, quantifies associated errors, and estimates transition probabilities and state-dependent distributions.

The combined GMM–HMM–KF framework offers a promising method for improving forecasts of intermittent solar resources, contributing to better management strategies for renewable energy in the Sahelian context.

## II. MATERIALS AND METHODS

### 1. Presentation of the Dakar Site

Dakar is located at the western tip of the Cape Verde Peninsula, on the Atlantic coast, at  $14.75^\circ$  N and  $-17.33^\circ$  W,

with an average elevation of 16 m (Fig.1). The area hosts several meteorological stations, including the measurement station of the International Center for Training and Research in Solar Energy (CIFRES) at the École Supérieure Polytechnique, Cheikh Anta Diop University. The station records global, direct, and diffuse solar radiation, ambient temperature, relative humidity, rainfall, and wind speed and direction.

This study uses global solar radiation, mean temperature, and relative humidity from the CIFRES station.

The length of the series extends on the one hand from October 1, 2016, to April 30, 2017, with an hourly time step; and on the other hand, from May 1, 2017, to September 30, 2017 with a step of 10 seconds. A Campbell Scientific model, the CR800 datalogger is used.

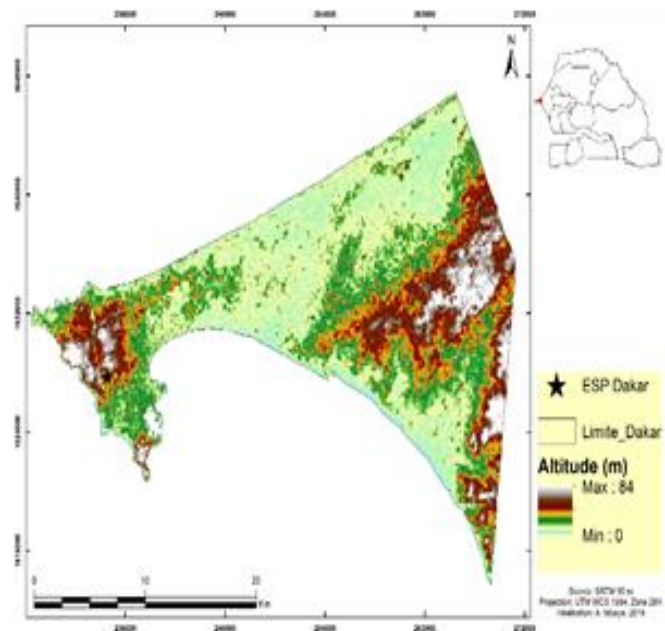


Figure 1: Geographical location of Dakar (Senegal)

### 1.1 Data Processing

The difference in sampling intervals reflects the laboratory's measurement requirements. To homogenize the measurement interval, we applied cubic interpolation in MATLAB to resample all data at 10 s. Fig.2 compares interpolated and hourly irradiance values; the close agreement validates the interpolation method. This approach can therefore be used to estimate irradiance at finer temporal scales.

After resampling, biased or erroneous measurements were removed. Missing values in solar radiation were reconstructed using linear regression, which showed strong correlation with the available data. These gaps resulted from a temporary connection failure between the pyranometer and the acquisition system.

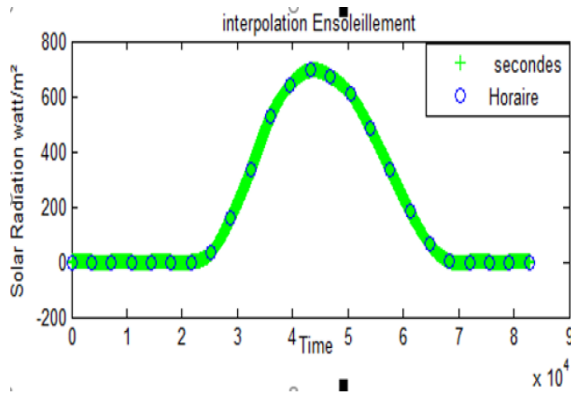


Figure 2: Cubic interpolation of solar irradiance data

## 2. Gaussian Mixture Model (GMM)

The mathematical tool used to estimate levels of variability and define a form of uncertainty regarding the classification of states within a database is probability theory. In probabilistic modeling approaches, mixtures of distributions are very useful. They are known for their ability to represent arbitrarily complex distributions with multiple modes.

To construct a GMM, it is necessary to choose a mixture component noticed by  $P(j)$  and generate a data point from the chosen component using the conditional event probability  $p(X/j)$ . Then, the event probability is given by:

$$p(X) = \sum_{j=1}^M p(X/j)P(j) \quad (1)$$

$p(X/j)$  represents the densities of the Gaussian components and  $P(j)$  the mixing parameters.

This method is generally used to perform unsupervised clustering because the clusters or groups are unknown in advance. They constitute the hidden states of the mixture model.

In the formulation of the GMM framework, if we assume that there is a set of  $K$  components, each value  $x$  is associated with an unobserved state, as follows:

- Data is generated using a set of  $M$  probability distributions  $p(X/j)$ .

- Each individual distribution is designed using a normal probability distribution so that:

$$P(X/\theta) = \varphi(X/\mu_m, \Sigma_m, \pi_m) \quad (2)$$

$P(X/\theta)$ : The probability of generating a value  $x$  under the  $m^{ième}$  model with:

$\mu_m$ : The average vector

$\Sigma_m$ : The matrix covariance data

$\pi_m$ : The probability of appearance.

$1 \leq m \leq M$ : The data is generated using a set of  $M$  probability distributions.

To find the parameters  $\theta = \left\{ \mu_m, \sum_m, \pi_m \right\}$  of the mixture model, we use the EM algorithm [23].

## 2.1 Parameters Estimation via the EM Algorithm

The EM algorithm derives its name from the fact that at each iteration, it performs two distinct steps:

First, it estimates the unknown data based on the observed data and the parameters determined during the previous iteration.

Second, it aims to maximize the likelihood using the estimates of the unknown data obtained during the previous step. Furthermore, it updates the value(s) of the parameter(s) for the next iteration. The algorithm also guarantees an increase in likelihood at each iteration, resulting in increasingly accurate estimators.

### 2.1.1 GMM calibration

The main challenge to overcome to ensure the proper functioning of the tool is certainly the calibration of the GMM model. Effective and optimal calibration of a GMM model consists of finding the parameters  $\theta$  using the EM algorithm.

To perform this calibration, we have observational data with a likelihood denoted by  $X = (x_1, x_2, x_3, \dots, x_N)$ , with a likelihood noted  $P(X/\theta)$  whose maximization  $\log P(X/\theta)$  is impossible.

This observational data includes global solar radiation, temperature, and relative humidity. Naturally, this solar radiation data is generally subject to many perturbations, resulting in significant variability. In this context, a thorough characterization of the solar resource is needed to detect these phenomena hidden in observational data.

In this case, we consider that there are hidden data  $Z = (z_1, z_2, \dots, z_N)$ , the knowledge of which will allow us to maximize the likelihood of the complete data  $P(X, Z/\theta)$ . Since the data  $Z$  is unknown, we evaluate the likelihood of the complete data by taking into account all available information.

Therefore, in the maximum likelihood approach, we maximize the probability expressions. Indeed, we will seek to maximize the probability  $P(X/\theta)$  and, equivalently but more computationally appropriately, the probability of the observed data  $P(X/\theta)$ , supplemented by a random vector  $Z$ . This random vector indicates, for each data point, the group to which it appears to belong for),  $N$  being the number of components in the mixture, the variable is an additional quantity associated with each of the.

This random vector indicates for each data point  $X_i$ , the group to which he appears to belong for  $Z = \{z_i\}$  pour  $1 \leq i \leq N$ ,  $N$  being the number of components of the mixture, the variable  $z_i$  is an additional quantity associated with each of the variable  $X_i$ .

The log-likelihood of the parameters  $\theta$  is expressed as:  $\text{Log } P(X, Z/\theta)$  where  $z_{im}$  represents the posterior probability that the point  $x_i$  was generated by the  $m^{\text{ième}}$  component of the mixture, according to the value of  $\theta$ .

In this case, instead of attempting to maximize the probability of the observed data  $p(X/\theta)$ , we try to maximize the joint distribution probability using the iterative EM (Expectation-Maximization) algorithm.

At the end of the maximization, we work with the logarithm of this quantity  $\log P(X, Z/\theta)$ . This quantity is also known as the complete probability.

Thus, ultimately, starting from a good initialization of the parameters  $\theta$ , the algorithm proposes to maximize the log-likelihood of the completed data by alternating two steps, E and M.

E-Step (Waiting Phase): Calculating the expected value of the hidden variable  $Z_i$  allows for an update of the posterior probability values. It allows us to evaluate the expected value of the log-likelihood based on the current parameter values  $\theta$ ; thus, the variable  $Z_{im}$  is calculated. This step is represented by equations (3), (4), and (5):

$$F(x) = e^{[-1/2(x_i - \mu_m)^T \sum_m^{-1}(x_i - \mu_m)]} \quad (3)$$

$$p(x_i / z_{im} = 1; \theta) = (2\pi)^{-\frac{1}{2}} \left| \sum_m^{-1} \right|^{-\frac{1}{2}} F(x) \quad (4)$$

$$\langle z_{im} \rangle = \frac{p(x_i / z_{im} = 1; \theta) \pi_m}{\sum_M p(x_i / z_i = 1; \theta) \pi_i} \quad (5)$$

M-Step (Maximization Phase): The "M" step takes the expected log-complete probability and maximizes it. The parameters  $\theta = \left\{ \mu_m, \sum_m^{-1}, \pi_m \right\}$  to be estimated are described

by the following three equations (6), (7), and (8):

$$\pi_m = \frac{\sum_{i=1}^N \langle z_{im} \rangle}{N} \quad (6)$$

$$\mu_m = \frac{\sum_{i=1}^N \langle z_{im} \rangle x_i}{\sum_{i=1}^N \langle z_{im} \rangle} \quad (7)$$

$$\sum_m^{-1} = \frac{\sum_{i=1}^N \langle z_{im} \rangle (x_i - \mu_m)(x_i - \mu_m)^T}{\sum_{i=1}^N \langle z_{im} \rangle} \quad (8)$$

### 3. Hidden Markov Model

Hidden Markov Models (HMMs) are one of the most powerful tools for modeling and analysis of sequential data [17]. They represent one of the most used probabilistic

approaches over the last three decades, such as recognition, speech synthesis, biology, planning, document indexing, image recognition, time series prediction, etc...[24]-[26]. These approaches are based on a probabilistic theory and allow for correctly modeling the temporal evolution of global solar radiation. The temporal evolution of such observation is a temporal phenomenon where chance notion intervenes. Chance involvement leads to random behavior in the data evolution that is also a function of the time  $X(t)$ . The random process in a time series manages the transition from one state to another, but the state of the system is not observable (it is hidden), we only see the emissions of the state. For that the HMM model random phenomena, which are supposed to be composed at a first level of a random process of transition between unobservable states (hidden) and, at a second level of a random process which, in each state, generates observable values (Observations). The articulation of these two levels give the HMM models great flexibility Models based on transitions between states are well-suited for the computation of the time series processes [3], [20]. These calculations are mainly based on principles and characteristics of the model.

### 3.1 Principle and Characteristics of the HMM

The state characterizes a Hidden Markov Model by the state transition matrix, the observation probability distribution matrix, and the initial states of the system. To define these first, two matrices from a dataset, it is necessary to distinguish between state variables and observations variables, listed as follows:

T: Number of observations

$Q = \{q_1, q_2, \dots, q_T\}$ : Sequences of observations

$O = \{o_1, o_2, \dots, o_T\}$ : Symbols of observations

$q_t \in X$  : Observations at time t

N: Number of states in the model

$S = \{s_1, s_2, \dots, s_N\}$ : States

$q_t \in S$  : States at time t

#### 3.1.1 State Transition Probability Matrix

The development of a model based on Markov chain theory requires the use of transition matrices [28]-[31]. For a given transition matrix, the transition probability from a state  $s_i$  at time t to the state  $s_j$  at time t+1 can be introduced by the following two conditions: "equation (9) and (10)"

$$a_{ij} = P[q_{t+1} = s_j / q_t = s_i] \quad 1 \leq i, j \leq N \quad (9)$$

$$a_{ij} \geq 0 \quad \text{and} \quad \sum_{j=1}^n a_{ij} = 1 \quad (10)$$

If these two conditions are met, the set of transition probabilities between the different components can be grouped into a matrix  $A = \{a_{ij}\}$ .

This matrix A is stochastic: the sum of all the elements  $a_{ij}$  of a row of the matrix is equal to 1. It is the basis for data

generation by Markov chains. It is a square of dimension  $N \times N$  because there are  $N$  possible states, where each row and column represents a possible state of the system. The elements of the transition matrix are represented as follows:

→  $q_{t+1}$  Future State

$$\downarrow q_t \quad A = \begin{bmatrix} \dots & q_1 & q_2 & q_3 \\ q_1 & a_{11} & a_{12} & a_{13} \\ q_2 & a_{21} & a_{22} & a_{23} \\ q_3 & a_{31} & a_{32} & a_{33} \end{bmatrix} \quad (11)$$

In a dataset, studying this matrix allows us to distinguish each of these probability groups, and also to deduce the stochastic nature of the hidden states over the time interval  $t$  to  $t+1$ . To detect these groups and conclude the process, comparing the coefficients  $i$  and  $j$  of the probabilities  $a_{ij}$  are essential. To ensure this comparison, we must meet these three conditions:

If  $i = j$ : we have this probability group  $a_{11}, a_{22}$  and  $a_{33}$  representing the elements of the main diagonal. Indeed, this diagonal has the highest probabilities, characterized by a stabilization of states during the period  $t$  to  $t+1$ .

If  $i \geq j$ : we have this probability group  $a_{21}, a_{31}$  and  $a_{32}$ , located below the main diagonal. This group experiences changes of state from deteriorating to a riskier state over the period  $t$  to  $t+1$ .

If  $i \leq j$ : we have this probability group  $a_{12}, a_{13}$  and  $a_{23}$  located below the main diagonal. This group experiences changes of state from improving to a less risky state over the period  $t$  to  $t+1$ .

### 3.1.2 Observation Probability Distribution

The observation matrix in a hidden Markov chain is often called the emission matrix or observation matrix. It represents the conditional probabilities, where the coefficient in row  $i$  and column  $j$  is the probability of emitting the observable  $o_k$  when the system is in the hidden state.

Let  $b_{ij}$  be the probability of observing the observable  $o_k$  when the stochastic process is in the hidden state  $s_i$ . This means that  $b_{ij} = P(o_k / q_i = s_i) \quad 1 \leq i, j \leq N \text{ and } 1 \leq k \leq T$

the set of observation probabilities  $b_{ij}$  constitutes the observation probability matrix  $B = \{b_{ij}\}$ . It is a square matrix of size  $N \times T$ , where  $N$  is the number of hidden states and  $T$  is the number of possible observables. For each hidden state, the sum of the probabilities of emitting all possible observables must equal 1.

The elements of the observation matrix are represented as follows:

$$B = \begin{bmatrix} \dots & q_1 & q_2 & q_3 \\ q_1 & b_{11} & 0 & 0 \\ q_2 & 0 & b_{22} & 0 \\ q_3 & 0 & 0 & b_{33} \end{bmatrix} \quad (12)$$

This observation matrix  $B$  is a diagonal matrix in which all elements off the main diagonal are zero. The recognition of these elements is described as follows:

#### ➤ Main diagonal

If  $i=j$ : the probabilities  $b_{ii} \neq 0$  represent the probability of not changing state. These large and high values indicate a high probability of remaining in a given state.

#### ➤ Off-diagonal

If  $i \neq j$ : we have the probabilities  $b_{ij}=0$  indicating the uncertainty and the errors of observation, and the probability that a hidden state does not produce the expected observation.

### 3.1.3 Initial State Distribution

$$\pi_i = P(q_i = s_i) \quad 1 \leq i \leq N \quad (13)$$

The set of all initial states

$$\pi = \{\pi_i\}$$

In summary, an HMM model is described by this model

$$\lambda = \{A, B, \pi\} \quad (14)$$

We will discuss how to adjust the model parameters  $\lambda$  to maximize  $P(O/\lambda)$ .

## 3.2 Training the HMM

Model parameters are estimated from classified or partially classified data, where temporal dependencies exist between variability levels. Each class contains one or more Gaussian components. Parameter estimation maximizes the likelihood of the observation sequence using the **Forward-Backward algorithm**. To determine the most probable sequence of hidden states, the **Viterbi algorithm** is employed.

### 3.2.1 Likelihood Computation

Calculating the likelihood of a sequence of  $T$  observations with respect to an HMM  $\lambda$ , it involves evaluating the probability of  $P(O/\lambda)$ . This calculation can be performed in several ways: naively, by direct computation, with a complexity of  $O(TN^T)$ , or efficiently, using the Forward and the Backward algorithm (Rabiner, 1989).

#### ➤ Forward Algorithm

To represent this Forward algorithm (or forward recurrence), it is necessary to define the Forward variables. A more efficient approach for evaluating  $P(O/\lambda)$ .

Let the defined variable  $\alpha_i(i) = P(o_1, o_2, o_3, \dots, o_T, q_t = i / \lambda)$  be the probability of the partial observation sequence  $o_1, o_2, o_3, \dots, o_T$ , and let  $i$  be the state number reached by the hidden process  $q$  at time  $t$ , given the model.

Algorithm:

- Initialization

$$\alpha_i(i) = \pi_i b_i(o_1), \quad 1 \leq i \leq N \quad (15)$$

- Recursion

$$\alpha_{t+1}(j) = \left[ \sum_{i=1}^N \alpha_t(i) a_{ij} \right] b_j(o_{t+1}), \quad (16)$$

$$1 \leq t \leq T-1 \quad \text{and} \quad 1 \leq j \leq N$$

- Termination

$$P(O/\lambda) = \sum_{i=1}^N \alpha_T(i) \quad (17)$$

With T observations and N states, this requires approximately  $N^2T$  operations.

#### ➤ Backward Algorithm

A more efficient approach for evaluating  $P(O/\lambda)$  in the reverse direction.

Define:

$$\beta_t(i) = P(o_{t+1}, o_{t+2}, o_{t+3}, \dots, o_T / q_t = i, \lambda) \quad (18)$$

As the probability of observations  $o_{t+1}$  with the sequence of states ending at state  $q_t = s_i$  for the HMM model.

Algorithm:

- Initialization

$$\beta_t(i) = 1, \quad 1 \leq i \leq N$$

- Recursion

$$\beta_t(i) = \sum_{j=1}^N a_{ij} b_j(o_{t+1}) \beta_{t+1}(j), \quad (19)$$

$$t = T-1, T-2, \dots, 1 \quad 1 \leq i \leq N$$

- Termination

$$P(O/\lambda) = \sum_{i=1}^N \pi_i b_i(o_1) \beta_1(i) \quad (20)$$

With T observations and N states, this requires approximately  $N^2T$  operations.

### 3.2.2 Segmentation Using the Viterbi Algorithm

Segmentation of observation sequences consists of finding the sequence of hidden states that maximizes the probability  $P(Q, O/\lambda)$  using Viterbi's algorithm. Two approaches are possible.

The first consists of accumulating the probabilities of maximum paths:  $\delta_t(i)$

The second allows us to keep track of the best sequences:  $\psi_t(i)$

- Initialisation

$$\delta_1(i) = \pi_i b_i(o_1), \quad 1 \leq i \leq N \quad (21)$$

$$\psi_1(i) = 0$$

- Recursion

$$\delta_t(j) = \max_{1 \leq i \leq N} [\delta_{t-1}(i) a_{ij}] b_j(o_t), \quad (22)$$

$$2 \leq t \leq T-1; \quad 1 \leq j \leq N$$

$$\psi_t(j) = \arg \max_{1 \leq i \leq N} [\delta_{t-1}(i) a_{ij}], \quad (23)$$

$$2 \leq t \leq T-1; \quad 1 \leq j \leq N$$

- Termination

$$P^* = \max_{1 \leq i \leq N} [\delta_T(i)] \quad (24)$$

$$q_T^* = \arg \max_{1 \leq i \leq N} [\delta_T(i)] \quad (25)$$

- Backtracking

$$q_t^* = \psi_{t+1}(q_{t+1}^*), \quad t = T-1, T-2, \dots, 1 \quad (26)$$

### 4. Modeling Using Steps the Kalman Filter

In this section, the problem of extracting a deterministic signal the raw, noisy one is processed. Solar resources are very noisy in nature, then the Kalman filter can be used to model deterministic data drowned in measurements and observations. For more understanding, a Kalman filter scheme is proposed in Fig.3 to contribute to the well understanding of an implementation towards the short-term forecast of intermittent energy production in the Sahelian zones. The process of the KF implementation is summarized in the flowchart Fig.3.

First, we process the provided measurements by eliminating erroneous values, replacing missing measurements, calculating the averages, etc. Then, the Kalman filter approach is performed using the retained data. The model run is based on these three well-separated stages. The first stage handles the initialization phase. At this stage, the process is at time  $t=0$ . At this time, the model does not see any measurement since it sees no measure. In this case, it seems logical to estimate its first step by the variable expectation and the associated convergence matrix. The second step consists of the proper prediction process. At this stage, the process is at the instant  $t$  at which the only known information is the initial estimate based on the knowledge of the process and the measurements up to instant  $t+1$ , i.e., the priori estimate. In the third stage, the stage of correction is propagated. At this level, measurements are provided at time  $t+1$  to correct the priori estimate to have a much more precise estimate, i.e., the posteriori estimate. After the correct performance of the KF model, the model calibration step is engaged. Indeed, to properly calibrate the model, the identification of the different parameters of the KF is necessary. For that, a well-known technique in the literature based on the EM algorithm described in [19] is used. Subsequently, two simulation scenarios are used to properly execute the KF model. The first scenario is the KF model based on the EM algorithm with the impact of exogenous parameters for a horizon of 20 minutes. The second is the KF model based on the EM algorithm without the involvement of the estimated parameters. Finally, the validity of the model is assessed through performance tests based on two instructions. The first is to confirm the model reliability if the tests are satisfactory, and if not, go back to review the estimated parameters. The flowchart described in Fig.3 summarizes the different steps for implementing a discrete Kalman filter. For a much more detailed description of the KF processing, one can consult my two papers [19], [35].

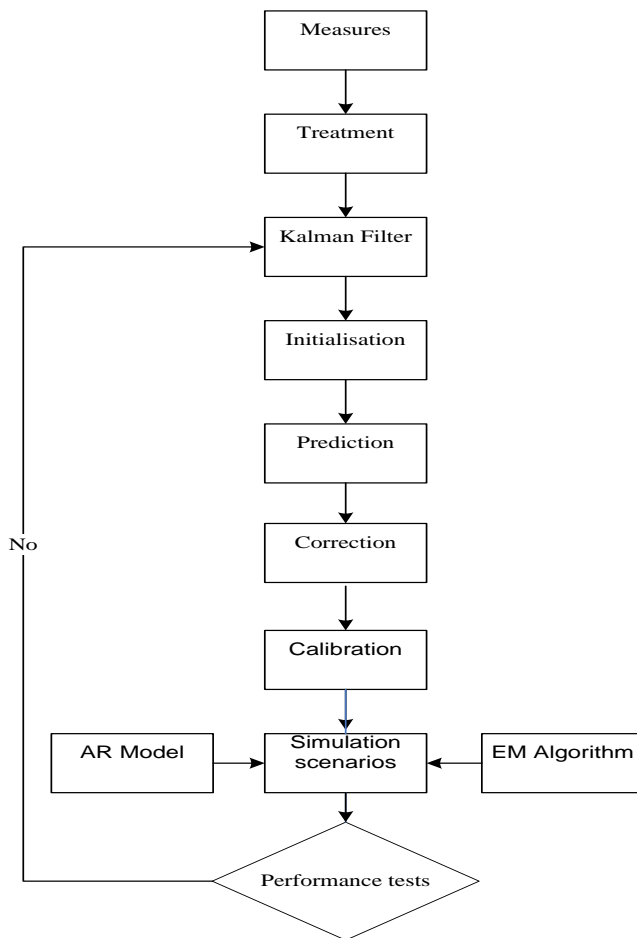


Figure 3: Iterative process of the Kalman Filter performing

### 5. Performance Criteria of the Model

In the context of predicting global solar radiation or photovoltaic power, several methods exist to assess the predictive accuracy of a model [32], [33], [34]. In this study, the evaluation is conducted using three statistical indicators: the Normalized Root Mean Square Error (NRMSE), the Normalized Mean Absolute Error (NMAE), and the Normalized Mean Bias Error (NMBE), defined as follows:

➤ **Root Mean Square Error (RMSE)**

The RMSE is a widely used metric that quantifies the deviation between predicted values and observed values. It represents the sample standard deviation of these differences. Normalizing the RMSE facilitates comparison across datasets or models with different scales, typically by dividing by the mean of observed values. The normalized RMSE (NRMSE) is often expressed as a percentage, as in Equation (27). It is important to note that NRMSE generally yields lower values than RMSE, effectively moderating the magnitude of nominal errors.

$$NRMSE = \frac{\sqrt{\frac{1}{N} \sum_{i=1}^N (P_i - \hat{P}_i)^2}}{\max(P_i) - \min(P_i)} \tag{27}$$

$P_i$  : The predicted (estimated) value,

$\hat{P}_i$  : The measured value

N denotes the number of data points considered.

➤ **Mean Absolute Error (MAE)**

The mean absolute error is a quantity often used to measure the difference between predictions and measurements. As with NRMSE, it is possible to use a relative form of this error by dividing it by the mean radiation value. The MAPE (Mean Absolute Percentage Error) or NMAE parameter is less sensitive to large errors, whereas the NRMSE heavily penalizes large discrepancies due to the squaring of the error. Thus, decreasing the NMAE will mean improving the prediction on average, while decreasing the NRMSE will mean limiting large prediction errors. The expression for the NMAE is given by equation (28):

$$NMAE = \frac{\frac{1}{N} \sum_{i=1}^N |P_i - \hat{P}_i|}{\max(P_i) - \min(P_i)} \tag{28}$$

➤ **Mean Bias (MBE)**

The MBE is defined as the mean algebraic difference between predicted and observed values. It is particularly informative for evaluating cumulative forecasting bias rather than instantaneous errors. A positive NMBE indicates that predictions systematically underestimate cumulative measurements, while a negative NMBE implies overestimation. Its computation is given by Equation (29).

$$NMBE = \frac{\frac{1}{N} \sum_{i=1}^N (P_i - \hat{P}_i)}{\max(P_i) - \min(P_i)} \tag{29}$$

### 6. Implementation Steps of the Hybrid Model

The purpose of developing a hybrid model in this study is to contribute to the improvement of the quality of the short-term forecast for intermittent energy production in the Sahelian zone. The methodology is summarized in the flowchart in Fig.4. First measurement assessment is performed to eliminate erroneous values, calculate averages, replace missing values, etc. The second step consists of applying the two probabilistic models (GMM and HMM) to the preprocessed data. However, in our previous work, a single forecasting model was applied to the whole measurements with a single probability distribution [2], [19], [20]. However, solar radiation generally undergoes many disturbances leading to notorious fluctuations in the recorded data. Indeed, the appearance of these fluctuations is explained by the meteorological conditions, which are due to exogenous parameters such as the cloud cover, the temperature, the wind, the humidity, etc. That’s why we would like to study the solar radiation variability and try to extract the different levels of fluctuation. To study variability levels, we use a Gaussian mixture model (GMM) and a Hidden Markov chain. Thus, the different states of the

models explain the variability levels of the variable. Here, we assume that each sub-process of the model is a Gaussian one, which leads us to want to extract the Gaussian mixture corresponding to these states, thanks to the mathematical tool GMM. Then, the use of an HMM allows for the extraction, from the mixture of Gaussians, the temporal dependencies between different variability levels using a Forward-Backward algorithm, and the best sequence of the states corresponding to the levels of variability, combined with the Viterbi algorithm. The Forward-Backward algorithm based on Expectation Maximization (EM) techniques help permit the finding of the necessary parameters of the HMM model [21]. In addition, calibrating an HMM also contributes to finding and numerically estimating the best parameters by the Viterbi algorithm for states estimation. The Viterbi algorithm, instead of maximizing the probability over all state sequences, tries to maximize the most probable states [22]. Then we apply a Kalman filter based on the EM algorithm to each retained best state to eliminate the noise of the signal. For a much more detailed reading of these algorithms, the reader is advised to consult [21]-[23]. Finally, we calculate the error rates of each state of the data from the experimental site. Different statistical indicators are used for. Statistical indicators are composed of the square root of the normalized root mean square error (NRMSE), the mean Absolute normalized error (NMAE), and the mean normalized bias error (NMBE). The flowchart depicted in Fig.4 summarizes the different steps for the hybrid model implementation.

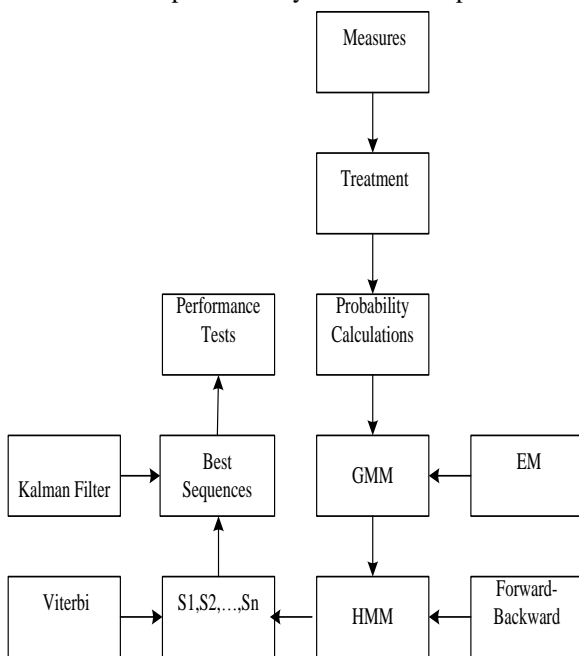


Figure 4: The complete hybrid model workflow

### III. Results and Discussion

#### 1. Hybrid Model Performance at the Dakar Site

The hybrid model was applied to real measurements of global solar radiation, temperature, and relative humidity at Dakar using Matlab software. Unlike the single Kalman filter approach, the hybrid model provides a probabilistic segmentation of the solar radiation process, capturing hidden states and variability.

##### 1.1 Probabilistic Quantification of Solar Variability

We apply a hidden Markov chain model to a dataset of actual measurements taken at the Dakar site. The model inputs global solar radiation, temperature, and relative humidity. The output is global solar radiation. The results obtained using the transition and observation matrices are presented in Table 1.

TABLE1. Distributions of the model states

| Transition Matrix   | Proportion Matrix  |
|---|--|
| $\begin{pmatrix} 0.916 & 0.084 & 0 \\ 0.087 & 0.826 & 0.087 \\ 0 & 0.075 & 0.925 \end{pmatrix}$ | $\begin{pmatrix} 0.3699 & 0 & 0 \\ 0 & 0.2851 & 0 \\ 0 & 0 & 0.3450 \end{pmatrix}$ |

##### 1.1.1 Results obtained from the Transition Matrix

Observing the 3x3 transition matrix reveals a clear separation of these three unequally distributed states. They are detectable according to the transition probability distributions  $a_{ij}$ .

According to the methodology adopted in section (2.2.1):

If  $i=j$ : we have this probability group  $a_{11}=0.916, a_{22}=0.826$  and  $a_{33}=0.925$ . It represents the elements of the main diagonal with the highest probabilities. This is explained by the fact that the evolution of global solar radiation is characterized by a fairly significant stability of the current state (of brightness) over the 20-minute horizon.

If  $i \geq j$ : we have this probability group  $a_{21}=0.087, a_{31}=0$  and  $a_{32}=0.075$  are located below the main diagonal. This group exhibits state changes, degrading towards a riskier state over the 20-minute horizon. This means that the evolution of global solar radiation is strongly impacted by exogenous variables such as temperature, relative humidity, etc. These variables naturally degrade the quality of global solar radiation.

If  $i \leq j$  we have this group of probabilities  $a_{12}=0.084, a_{13}=0$  and  $a_{23}=0.087$  are located above the main diagonal, these probabilities are higher than those located below the main diagonal. This shows that the evolution of global solar radiation is less impacted by exogenous variables. We can confirm that there is an improvement in the quality of the radiation over the 20-minute horizon.

Furthermore, some of these off-diagonal transition probabilities are zero. This shows that the conditions for transitioning between the states in question is practically nonexistent: it is very difficult to move from one state to another.

In short, the values located on the main diagonal have the highest probabilities. Consequently, the evolution of global solar radiation is more stable (almost no impact). Conversely, the probabilities located above the main diagonal are higher (less impacted) than those located below the main diagonal.

**1.1.2 Observation Matrix Results**

By adopting the methodology used in section (2.2.1), the results obtained with the observation matrix are analyzed and interpreted as follows:

If  $i \neq j$ : the probabilities  $b_{ij} = 0$ , representing the errors and uncertainties in the evolution of global solar radiation, it is characterized by a fairly significant instability in the present state. However, evaluating the impact rate of these exogenous variables on the evolution of global solar radiation will be very complicated, as it is impossible to separate the hidden states from the observations.

If  $i = j$ : we have this group of probabilities  $b_{11} = 0.3699$ ,  $b_{22} = 0.2851$  and  $b_{33} = 0.3450$  representing the elements of the main diagonal, these probability values clearly show that it is more likely to remain longer in state 1 than in the other two states, with a probability of 37%. Next, the probability of remaining in state 3 is 34%, and finally, the probability of remaining in state 2 is 28%.

**1.2 Detection of Variability Levels**

We perform the analysis on a Hidden Markov Chain-based on the visual analysis of global solar radiation sampled in 20-minute intervals (Fig.5).

Based on the statistical behavior of the different parameters, a simple regime change process between solar classes is proposed by the Viterbi algorithm. This algorithm, instead of maximizing the probability over all possible states sequences, maximizes the probability only over the most probable state sequences. Indeed, the analysis of the temporal sequence of the classes leads us to believe that the days of solar radiation are governed by a Hidden Markov Chain. By observing the dynamic evolution of global solar radiation and segmenting the levels of variability (Fig.5), it is possible to detect these hidden phenomena within the radiation.

Following the dynamic evolution of global solar radiation (blue curve), we observe that solar radiation is generally subject to many perturbations. These perturbations generate significant spatiotemporal variability in the process. The emergence of this variability is explained by changing meteorological conditions over time. Therefore, we perform data segmentation to extract the phenomena hidden within the data.

On the radiation segmentation curve (black curve), we detect three levels of variability in global solar radiation. These levels correspond to a state of very sunny clear skies (state 3), another state describing a partly cloudy sky (state 1), and a state corresponding to a very cloudy and rainy sky (state 2). Furthermore, we observe that certain days follow the same types of fluctuations, determining the same sequences of states. Following this process, we evaluate the impact rate of these exogenous variables on each of these sequences of states.

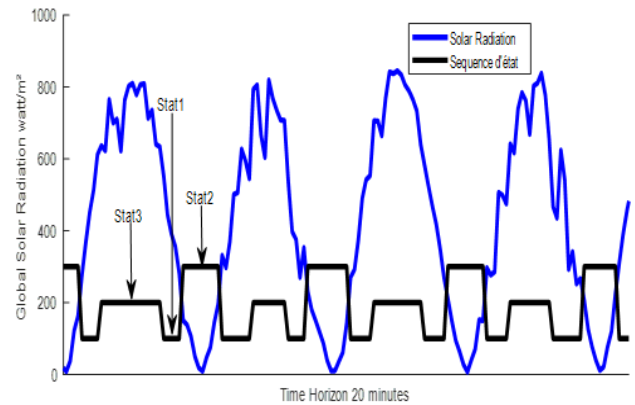


Figure 5: Three levels of the global solar radiation variability

**1.3 Characterization of Sky Conditions in Dakar**

In this section, we interpret the results of the characteristics of the state of the sky in the Sahelian environment, shown in Table 2.

TABLE 2. Characteristics of the state of the sky at Dakar

| States | states of the sky                 | State Sequence  |
|--------|-----------------------------------|---|
| State1 | Lightly covered with 0.98% impact | $\begin{pmatrix} 0.916 & 0.084 & 0 \\ 0.087 & 0.826 & 0.087 \\ 0 & 0.075 & 0.925 \end{pmatrix}$ |
| State2 | Covered with 11.98% impact        |   |
| State3 | Very sunny                        |   |

The transition and observation matrices confirm three well-separated states, allowing calculation of the impact of meteorological parameters:

State 1: Lightly covered sky, 0.98% impact

State 2: Overcast, 11.98% impact

State 3: Very sunny, negligible impact

High main-diagonal probabilities indicate stable state persistence, confirming the relevance of state-based segmentation for accurate forecasting.

**1.4 Kalman Filter Model Application**

The Kalman filter was applied to the segmented data for short-term forecasting. Correlation analysis between measured and predicted values yielded ( $R = 0.9912$ ), indicating strong agreement. The inclusion of temperature and humidity had minimal effect on performance over a 20-minute horizon (Table 3).

**1.4.1 Evolution of Measured Data and those Predicted by the Kalman Filter**

Fig.6 shows the evolution of the values observed at the study site (in yellow) and those predicted by the Kalman filter model (with and without the impact of atmospheric parameters) based on the EM algorithm (green curve). It can be seen that the data predicted by the two simulation scenarios correspond well to the observations.

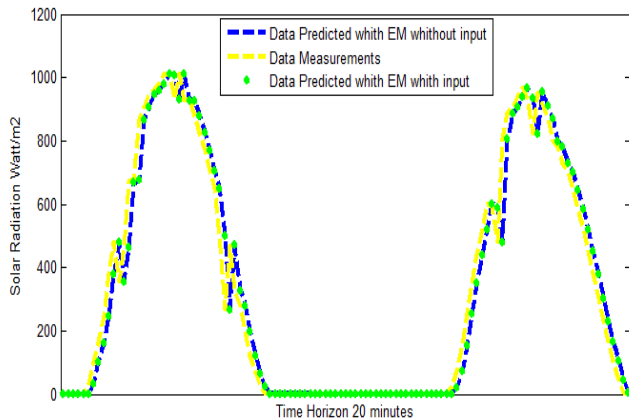


Figure 6: Evolution of measured data and data predicted by the filter model

**1.4.2 Correlation between Measurements and Predictions**

Fig.7 presents the correlation between the values measured on the study site and those predicted by the filter model based on the EM algorithm over a horizon of 20 minutes. We notice a good distribution of the points around the first diagonal and the value of the correlation coefficient  $R=0.9912$ , which tends almost towards 1, so we have a good agreement between the predicted data and the real measurements.

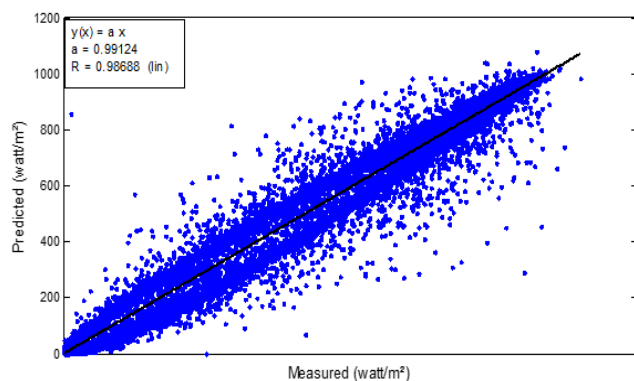


Figure 7: Correlation between measurements and predictions from the Filter via EM

**1.4.3 Impact of the Temperature and the Relative Humidity on Model Performances**

We will evaluate the performance of Kalman filter models based on the EM algorithm with and without the impact of exogenous parameters over a 20-minute horizon (see Table 3).

TABLE 3. Model performance over a 20 minutes horizon

| Kalman Filter       | NRMSE | NMBE   | NMAE  | No time (minutes) |
|---------------------|-------|--------|-------|-------------------|
| EM <sub>input</sub> | 0.049 | -0.007 | 2.718 | 20                |
| EM                  | 0.048 | 0.004  | 2.711 |                   |

Table 3 presents, on the one hand, the results of the model based on the EM<sub>input</sub> algorithm with impact (NRMSE of 4.9%, NMAE of 0.272% and NMBE of -0.7%) and, on the other hand, those of the EM model without impact (NRMSE of 4.8%, NMAE of 0.271% and NME of 0.4%). The relative differences between the values of NRMSE, NMBE, and NMAE are respectively equal to 0.1%, 0.001% and 0.3%. The involvement of Temperature and Relative humidity has a very weak influence on the model performances over a 20-minute horizon. The best performance was obtained with the Kalman filter based on the EM algorithm without the impact of the temperature and the Relative humidity.

**1.5 Comparison of Hybrid Model and Kalman Filter Performance**

TABLE4. Comparative study of the performances of the Hybrid model and that of Kalman Models

| Models        | NRMSE  | NMAE   | NMBE   |
|---------------|--------|--------|--------|
| State1        | 0.0093 | 0.0439 | 0.0006 |
| State2        | 0.0092 | 0.0431 | 0.0005 |
| State3        | 0.0096 | 0.0436 | 0.0008 |
| Kalman Filter | 0.048  | 2.718  | 0.004  |

The comparative analysis of the results presented in table 4 shows that the three states of the hybrid model [state1: NRMSE=0.0093, NMAE=0.044 and NMBE=0.0006, state2: NRMSE=0.0092, NMAE=0.0431 and NMBE=0.0005 and state3: NRMSE=0.0096, NMAE=0.0436 and NMBE=0.0008] provide better performance than the single Kalman filter [NRMSE=0.048, NMBE=2.718 and NMAE=0.004] according to each of the three criteria. In reality, the error found for the Kalman filter is almost twice larger than those found for the hybrid model. The results clearly show that the segmentation into several states gives best performance with a significant reduction of the

estimated error rates. Results obtained by the Kalman filter without prior decomposition into a sequence of states gave quite high errors. This is mainly due to the fact that the data are very variable in nature, and the underlying process is often determined by a set of probability laws. And therefore, it is not easy to calibrate the filter with optimal input parameters that can give results with low error rates. When the segmentation is carried out, the states correspond to a certain law of which we can know the exact parameters. In this case, calibrating the Kalman filter is straightforward. Therefore, it is much more efficient to apply the procedure at different levels of variability rather than applying it all at once to the entire dataset. This is because different statistical properties can be identified in the data. We can thus confirm the importance of using a hybrid forecasting model to obtain optimal results.

## V. Conclusion

This work presents a comprehensive hybrid model combining GMM, HMM, and Kalman filtering to improve short-term solar radiation forecasting in Dakar, Senegal. The methodology effectively segments solar radiation data into well-defined variability states, enabling precise characterization and modeling of the stochastic solar resource influenced by meteorological conditions. Performance evaluation over a 20-minute horizon confirms that the hybrid approach markedly reduces prediction errors (NRMSE= 0.0093, NMAE= 0.044, and NMBE= 0.0006) compared to a single Kalman Filter (NRMSE= 0.048, NMBE= 2.718, and NMAE= 0.004), highlighting the importance of state-based segmentation. These results emphasize the hybrid model's potential contribution to enhancing the reliability and accuracy of intermittent solar energy forecasts, facilitating better integration and planning of photovoltaic power in the Sahelian region. Future work could extend this framework with real-time implementation and integration of additional meteorological variables to further optimize forecasting accuracy.

## REFERENCES

- [1] P. Lauret, M.H. Diagne, M. David, A. Rodler, M. Muselli, C. Voyant, «A Bayesian model committee approach to forecasting global solar radiation», In: World renewable energy forum, WREF2012, including world renewable energy and Colorado renewable energy society (CRES) annual conference, 4354–4359, (2012).
- [2] J.M. Vindel and J. Polo, «Markov processes and Zipf's law in daily solar irradiation at earth's surface», Journal of Atmospheric and Solar Terrestrial Physics, 107, pp.42-47, (2014).
- [3] D.W. Vander Meer, «comment on verification of deterministic solar forecasts: Verification of probabilistic solar forecasts», Sol Energy 2020. <http://dx.doi.org/10.1016/j.solener.2020.04.015>.
- [4] P. Lauret and al, «Probabilistic Solar Forecasting Using Quantile Regression Models Forecasting», Energies 2017, 10, 1591; doi: 10.3390/en10101591.
- [5] T. Hong and S. Fan, «Probabilistic electric load forecasting: a tutorial review», International Journal of Forecasting, (2016); doi.org/10.1016/j.ijforecast.2015.11.011.
- [6] D.W. Vander Merr, J. Widen and J. Munkammar «Review on probabilistic forecasting of photovoltaic power production and electricity consumption Renewable and Sustainable Energy Reviews, Volume81, Part1, 2018, PP-1484-1512, ISSN1364-0321, (2018); doi.org/10.1016/j.rser.2017.05.212.
- [7] G.P. Zhang and al, «Time Series Forecasting using a hybrid ARIMA and neural network model», Neurocomputing, Volume 50, 2003, Pages 159-175, ISSN09252312, [https://doi.org/10.1016/S0925-2312\(01\)00702-0](https://doi.org/10.1016/S0925-2312(01)00702-0).
- [8] C. Voyant, M. Muselli, C. Paoli and M.L. Nivet, «Numerical weather prediction (NWP) and hybride ARMA/ANN model to predict global solar radiation», Energy 2012; 39(1):341-341-355.
- [9] W. Ji and K.C. Chee, «Prediction of hourly solar radiation using a novel hybrid model of ARMA and TDNN», Solar Energy, 85(5), 808-817, (2011).
- [10] G. Reikard and al, «Predicting solar radiation at high resolutions: A comparison of time series forecasts», (March 2009), Solar Energy 83 (3): 342-349, DOI: 10.1016/j.solener.2008.08.007.
- [11] M. Diagne and al, «Postprocessing of solar irradiance forecasts from WR Fmodelat Reunion Island », Solar Energy, Volume105, July2014, Pages99-108, <https://doi.org/10.1016/j.solener.2014.03.016>.
- [12] A. Mellit, M. Benghanem and M. Bendekhis, «Artificial neural network model for prediction Solar radiation data: Application for sizing stand-alone photovoltaic power system », July 2005, IEEE Xplore, Conference: Power Engineering Society General Meeting, (2005), DOI:10.1109/PES.2005.1489526.
- [13] S.A.P. Kani and al, «Very short-term wind speed prediction: A new artificial neural network-Markov chain model », Energy Conversion and Management 52 (1):738-745, (2011).
- [14] F.O. Hocaoglu and al, «A novel hybrid (Mycielski Markov) model for hourly solar radiation Forecasting, Renewable Energy, Volume 108, (2017), pages 635643, <https://doi.org/10.1016/j.renene.2016.08.058>
- [15] Shuai Li and al, «Typical Solar radiation year construction using k-means clustering and discrete-time Markov chain», Applied Energy, Volume 205, 1 November 2017, Pages720-731.
- [16] Duda R. O., Hart P. E., «Pattern Classification and Scene Analysis », John Wiley and Sons, New York, USA, 1973.
- [17] L.R. Rabiner, «A tutorial on Hidden Markov Models and selected and selected applications in speech recognition», Proc. IEEE, vol. 77, pp.257-286, (1989).
- [18] B.O. Ngoko, H. Sugihara and T. Funaki, «Synthetic generation of high temporal resolution solar radiation data using Markov models », Sol. Energy 103, 160-170, (2014).
- [19] A.Mbaye, J. Ndong, M.L. Ndiaye and al, «Kalman filter model as a tool for short-term forecasting of solar potential: case of the Dakar site», EDP Science, vol.57, p 2267 (2018).
- [20] A.Mbaye, M.L. Ndiaye, D.M. Ndione and al, «ARMA model for short term forecasting of solar potential: application to a horizontal surface on Dakar site», OAJ Mater Device 4 (1):1-8, (2019).
- [21] L. R. RABINER and B.H. JUANG, «An introduction to hidden Markov Models», IEEE ASSP Magazine, p.4-16, (1986).
- [22] Forney G. D, « The Viterbi Algorithm, Proceedings of the IEEE », vol 61, no 3, pp 263-27, 1973.
- [23] Dempster A. P., Laird N. M., and Rubin D. B., « Maximum likelihood from incomplete data via the EM algorithm », Journal of the Royal Statistical Society B, 39:1-38, 1977.
- [24] N. Morgan and H. Boulard, «Continuous Speech Recognition: An Introduction to the Hybrid HMM /Connectionist Approach», IEEE Signal Processing Magazine, Vol. 12, n°3, pp. 25-42, Mai 1995.
- [25] W. PIECZYNSKI, « Chaînes de Markov triplets et segmentation des images », Chapitre4 ; PP127, (janvier 2009).
- [26] W. Pieczynski, Modèles de Markov en traitements d'images Markov models in image processing, Traitement du Signal », Vol. 20, No. 3, pp.255-278, (2003).
- [27] P. Brémaud and al, «Initiation aux Probabilités et aux chaînes de Markov », Springer, (2009).
- [28] F.C. Kaminsky, R.H. Kirchoff, Syu C.Y. Manwell J.F. (1990b), A comparison of alternative approaches for the synthetic generation of a wind speed time series». Wind Engineering, 9ème symposium, 1-8.
- [29] Kirchoff R.H., Kaminsky F.C., Syu C.Y., (1988), «A Markov Chain analysis of wind speed at windsor, Massachusetts». Wind Engineering, 5, 9-16.
- [30] J.S.E. Moon, S.B. Ryoo, J.G. Know, (1994), «A Markov chain model for daily precipitation in South Korea». International Journal of Meteorology, 4, 1009-1016.

- [31] P.Sparis ,J.Antonogiannakis, D.Papadopoulos, (1995),«Markov Matrix coupled approach to wind speed and direction simulation», Wind Engineering, Vol 19(3), 121-133.
- [32]Ted Soubdhan,Joseph Ndong andal,«A robust forecasting framework based on the Kalman filtering approach with a twofold parameter tuning procedure: Application to solar and photovoltaic prediction»,SolarEnergy, 2016; 131:246 -259.
- [33]E.Lorenz, J.Remund, S.C.Muller, W.Traunmuller, G.Steinmaurer, D.Pozo andal, «Benchmarking of different approaches to forecast solar irradiance»,24<sup>th</sup> European Photovoltaic Solar Energy Conference Hamburg, Germany, vol. 21, 25, (2009).
- [34] H. Jiang, Y. Dong and L. Xiao, «A multi stage intelligent approach based on an ensemble of two-way interaction model for forecasting the global horizontal radiation of India», Energy Conversion and Management, vol.137, p 142 (2017).
- [35] A. MBAYE, M.L. NDIAYE, J.Ndong and P.A.S.Ndiaye, «Impact of meteorological parameters on short-term forecasting: Application to the Dakar site », in Proceedings of the 2019 IEEE 2nd International Conference on Power and Energy Applications 2019 (ICPEA 2019), Singapore, April 2019.

---

**Important:** Articles are published under the responsibility of authors, in particular concerning the respect of copyrights. Readers are aware that the contents of published articles may involve hazardous experiments if reproduced; the reproduction of experimental procedures described in articles is under the responsibility of readers and their own analysis of potential danger.

### Reprint freely distributable – Open access article

**Permissions – Important: all materials in this article may be freely reused (figures, tables, ...) without any need to ask permission or to pay any fee. It is simply asked to refer to the article.**

Materials and Devices is an Open Access journal which publishes original, and peer-reviewed papers accessible only via internet, freely for all. Your published article can be freely downloaded, and self archiving of your paper is allowed and encouraged! Put your article as soon as possible on your personal sites, institutional sites, etc!

We apply « the principles of transparency and best practice in scholarly publishing » as defined by the Committee on Publication Ethics (COPE), the Directory of Open Access Journals (DOAJ), and the Open Access Scholarly Publishers Organization (OASPA). The journal has been designed so that it can be accepted by DOAJ, and we are happy to inform you that this is the case now.

Copyright on any article in *Materials and Devices* is retained by the author(s) under the Creative Commons (Attribution-NonCommercial-NoDerivatives 4.0 International (CC BY-NC-ND 4.0)), which is favourable to authors.



**Aims and Scope of the journal :** the topics covered by the journal are wide, Materials and Devices aims at publishing papers on all aspects related to materials (including experimental techniques and methods), and devices in a wide sense provided they integrate specific materials. Works in relation with sustainable development are welcome.

The journal publishes several types of papers : A: regular papers, L : short papers, R : review papers, T : technical papers, Ur : Unexpected and « negative » results, Conf: conference papers, M: methods; and O: Opinion papers.

(see details in the site of the journal: <http://materialsanddevices.co-ac.com/submitarticle.html> )

**Important: all submitted articles, fulfilling above indications, are evaluated by peers from a pure scientific point of view! The editor-in-chief does not take any right of censorship, whether on the basis of the subject of the article, or the strength of the “profile of the authors”, their reputation, or other. We do not take any action to mechanically optimize the impact factor of the journal, for example by analyzing the forecast number of citations of the article based on the number of scientists working in the field, or fashion effects, or other.**

We want to maintain Materials and Devices Open Access and free of charge thanks to volunteering, the journal is managed by scientists for science! You are welcome if you desire to join the team!

Feel free to contact us! [contact@co-ac.com](mailto:contact@co-ac.com)